Inorganic Chemistry

Article

pubs.acs.org/IC

Structural Parameters of Pr_3MgNi_{14} during Hydrogen Absorption–Desorption Process

Kenji Iwase,*[,†] Naoyoshi Terashita,[‡] Kazuhiro Mori,[§] and Toru Ishigaki[†]

[†]Frontier Research Center for Applied Sciences, Ibaraki University, 162-1 Shirakata, Tokai, Naka, Ibaraki 319-1106, Japan

[‡]Japan Metals & Chemicals Co., Ltd., Nishiokitama-gun, Yamagata 999-1351, Japan

[§]Research Reactor Institute, Kyoto University, 2-1010 Asashiro-nishi, Kumatori, Sennan, Osaka 590-0494, Japan

ABSTRACT: Structural parameters of Pr_3MgNi_{14} after a cyclic hydrogen absorption–desorption process were investigated by X-ray diffraction. Pr_3MgNi_{14} consisted of two phases: 80% Gd_2Co_7-type structure and 20% $PuNi_3$-type structure. The pressure–composition (P–C) isotherm of Pr_3MgNi_{14} indicates a maximum hydrogen capacity of 1.12 H/M (1.61 mass %) at 298 K. The cyclic property of Pr_3MgNi_{14} up to 1000 cycles was measured at 313 K. The retention rate of the sample was 87.5% at 1000 cycles, which compares favorably with that of $LaNi_5$. After 1000 cycles, the expansions of lattice parameters a and c and the lengths along the c-axes of the $PrNi_5$ and $PrMgNi_4$ cells of the Gd_2Co_7-type structures were 0.20%, 1.26%, 0.47%, and 3.68%, respectively. The metal sublattice expanded anisotropically after the cyclic test. The isotropic and anisotropic lattice strains can be refined by Rietveld analysis. The anisotropic and isotropic lattice strains were almost saturated at the first activation process and reached values of 0.2% and 0.1%, respectively, after 1000 cycles. These values are smaller by 1 order of magnitude than those of $LaNi_5$.

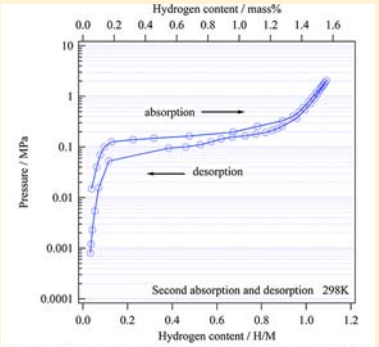

P-C isotherm of Pr_3MgNi_{14} was measured at 298 K.

1. INTRODUCTION

$RNi_{3-3.8}$ intermetallic compounds (R = rare earth) consist of $MgZn_2$-type and $CaCu_5$-type cells stacked along the c-axis and $PuNi_3$-, Ce_2Ni_7-, Gd_2Co_7-, Sm_5Co_{19}-, and Ce_5Co_{19}-type superlattice structures are known to exist. Among them, $CeNi_3$, Ce_2Ni_7, La_2Ni_7, La_5Ni_{19}, and Gd_5Ni_{19} have been investigated as hydrogen storage materials.[1−5]

Yasuoka et al. investigated the cyclic discharge capacity of $(Mm_{0.83}Mg_{0.17})Ni_{3.1}Al_{0.2}$ (Mm = mischmetal, an alloy of rare-earth elements), with the Ce_2Ni_7-type structure as a negative electrode of Ni–metal hydride (MH) batteries.[6] The alloy showed a better cyclic stability and a higher electrochemical capacity than those of $MmNi_5$-based alloys with the $CaCu_5$-type structure. Zhang et al. measured the pressure–composition (P–C) isotherm of the La_4MgNi_{19}–H_2 system at 298–338 K.[7] The hydriding and dehydriding enthalpies were determined to be −32.1 and 31.5 kJ/mol H_2, respectively, from the van't Hoff plot, which are close to those for the $LaNi_5$–H_2 system.[8] Liu et al. reported cyclic properties of hydrogen absorption–desorption in $(La,Mg)_5Ni_{19}$.[9] After 30 cycles, the hydrogen capacity decreased to 89% from the first cycle.

The crystal structures of La_4MgNi_{19} and its hydrides were investigated by Nakamura et al. using in situ X-ray diffraction (XRD) and in situ neutron diffraction.[10] La_4MgNi_{19} consisted of five phases: 51% Ce_5Co_{19}-type, 19% Pr_5Co_{19}-type, 16% Gd_2Co_7-type, 10% $CaCu_5$-type, and 4% Ce_2Ni_7-type structures. The Mg atom was assumed to substitute for the La sites in the $MgZn_2$-type cell in these structures. The expansions of a and c of the full hydride phase with the Ce_5Co_{19}-type structure were 7.3% and 8.8%, respectively, from the original alloy; the unit cell of the hydride phase expanded almost isotropically.

It is possible to use Rietveld refinement software to analyze the anisotropic line broadening of the powder diffraction profile and the direction of anisotropic peak broadening, thus refining the values of isotropic and anisotropic lattice strains. Nakamura et al. investigated peak broadening in XRD profiles of $LaNi_5$ and $LaNi_{5-x}M_x$ (M: Mn, Fe, Cu, Al) before hydrogenation, after activation, and after 1000 absorption–desorption cycles, and they were able to determine the anisotropic peak-broadening axis.[11]

In the present study, we investigated the P–C isotherm, the cyclic hydrogen absorption–desorption properties, and the structural parameters of Pr_3MgNi_{14} after hydrogenation. The P–C isotherm of Pr–Ni binary alloy with superlattice structure was reported.[12] Approximately 30% of the maximum hydrogen capacity remained after the first desorption process. It is interesting to elucidate how lattice strain and hydrogen capacity are changed by the Mg substitution and how the lattice strain is related to the cyclic hydrogen absorption–desorption properties. We focused on the lattice expansion of the unit cell, as well as on the $MgZn_2$-type and $CaCu_5$-type cells after the cyclic tests. The isotropic and anisotropic lattice strains are also presented.

Received: August 8, 2012
Published: October 17, 2012

2. EXPERIMENTAL SECTION

A Pr-Mg-Ni ternary alloy was prepared by induction melting of Pr, Mg, and Ni metals (99.9%) in a high-purity alumina crucible under a 0.07 MPa helium atmosphere. The Pr-Mg-Ni ingot was then annealed at 1343 K for 10 h under argon atmosphere. The chemical analysis of the annealed sample was conducted using inductively coupled plasma analyzers, which indicated a chemical composition of $Pr_{2.95}Mg_{1.04}Ni_{13.66}$.

The sample for the $P-C$ isotherm measurement was heated in vacuum at 413 K for 1 h and then held at measuring temperatures for 1 h in a stainless-steel container. The $P-C$ isotherm was measured using Sieverts' method. Hydrogenation was carried out at room temperature at 2.0 MPa, and then dehydrogenation was carried out using a rotary pump at 373 K for 1 h. After these processes had been performed three times, the cyclic test was carried out automatically using a $P-C$ isotherm machine. Fresh hydrogen gas was introduced for each cycle. The purity of the hydrogen gas was 99.99999%. After each cycle, the sample was evacuated using a rotary pump. The cyclic properties were measured at 313 K up to 1000 cycles.

The powder sample for XRD measurement was sieved to a particle size of <20 μm. The XRD data were collected in step-scan mode using a Rigaku Ultima IV diffractometer. Cu Kα radiation monochromatized by a curved graphite crystal was used. The structural parameters were refined using the Rietveld refinement program RIETAN-2000.[13,14] The reliability of the fitting was judged from the goodness-of-fit parameter S, defined as $S = R_{wp}/R_e$, where R_{wp} is the residue of the weighted pattern and R_e is the statistically expected residue. The peak-shape function was used a pseudo-Voigt function containing Gaussian and Lorentzian functions.[15,16] The anisotropic lattice strain was calculated using the Lorentzian parameter Y_e.

3. RESULTS

3.1. Crystal Structure of Pr_3MgNi_{14}. The XRD profile of Pr_3MgNi_{14} in the 2θ region between 3° and 15° is shown in Figure 1. Three superlattice reflections of the Ce_2Ni_7-type

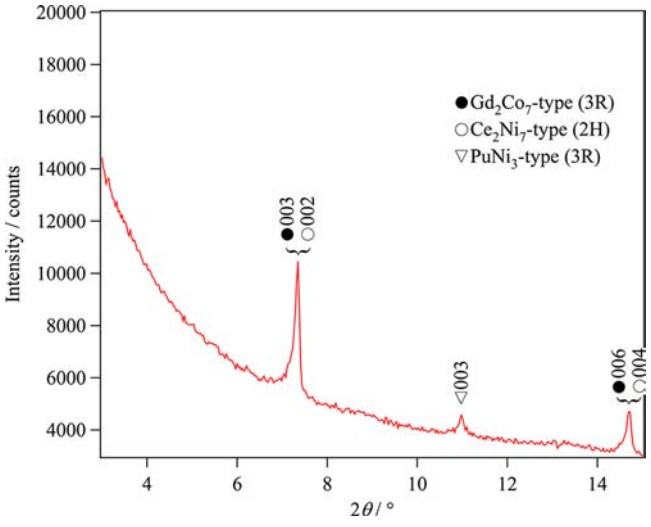

Figure 1. X-ray diffraction (XRD) profile of Pr_3MgNi_{14} in a low-angle region.

structure (002 and 004), the Gd_2Co_7-type structure (003 and 006), and the $PuNi_3$-type structure (003) were observed. These three peaks correspond to d = 1.2, 0.80, and 0.60 nm, respectively. An initial structural model based on two phases of the Ce_2Ni_7-type structure (space group $P6_3/mmc$) and the $PuNi_3$-type structure was adopted for the Rietveld refinement. The calculated pattern did not fit well with the observed pattern; S = 4.8. Then, another two-phase model of the Gd_2Co_7-type (space group $R\bar{3}m$) and $PuNi_3$-type structures was used. The crystal structure of the Gd_2Co_7-type is shown in Figure 2. The model contains two different Pr sites, Pr1 and

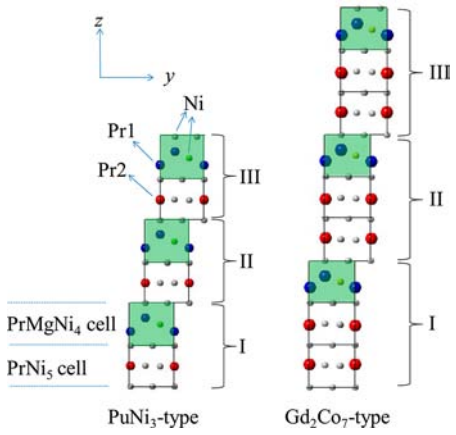

Figure 2. $PuNi_3$-type (3R) and Gd_2Co_7-type (3R) structures.

Pr2, at the 6c-site located in the A_2B_4 and AB_5 cells, respectively. The substituted Mg atoms were initially assumed to be located at both Pr1 and Pr2, which gave an S value of 1.9. Further modification of the model, in which the Mg atoms were located only at the Pr1 site, gave better agreement with the observed data and the S value was 1.6. The Rietveld refinement pattern is shown in Figure 3. Mass fractions of the Gd_2Co_7-type

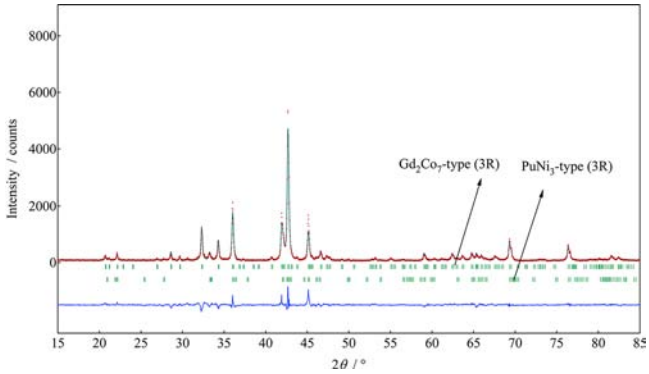

Figure 3. Rietveld refinement pattern of XRD data for the Pr_3MgNi_{14} sample. The sample contains two phases of Gd_2Co_7-type and $PuNi_3$-type structures.

and $PuNi_3$-type structures were 80% and 20%, respectively. The refined structural parameters of the Gd_2Co_7-type structure are listed in Table 1. The refined lattice parameters of the coexisting $PuNi_3$-type structure were a = 0.4981(1) nm and c = 2.4104(5) nm.

3.2. P–C isotherm of Pr_3MgNi_{14}. Figure 4 shows the $P-C$ isotherm of Pr_3MgNi_{14} for the first and second absorption–desorption processes at 298 K. The first absorption–desorption isotherm was measured with no other pretreatment for activation. The plateau region was observed between 0.14 H/M and 1.00 H/M. The first absorption and desorption plateaus were at P_{abs} = 0.61 MPa and P_{des} = 0.14 MPa, respectively. The hysteresis factor, Hf = $\ln(P_{abs}/P_{des})$, was 1.47, which was slightly larger than that of $LaNi_5$ (Hf = 1.25). The maximum hydrogen capacity reached 1.12 H/M (1.61 mass %) at 2 MPa. Before the second absorption–desorption process, the sample was

dx.doi.org/10.1021/ic301743p | Inorg. Chem. 2012, 51, 11805–11810

Table 1. Structural Parameters of Gd_2Co_7-Type Phase[a]

atom	site	g	x	y	z	B ($\times 10^{-2}$ nm^2)
Pr1	6c	1.0	0	0	0.0525(1)	1.2(1)
Pr2	6c	0.5	0	0	0.1517(1)	0.7(1)
Mg	6c	0.5	0	0	0.1517 (1)	0.7(1)
Ni	18h	1.0	0.500(1)	0.500(1)	0.1111(1)	0.7(2)
Ni	9e	1.0	1/2	0	0	0.3(2)
Ni	6c	1.0	0	0	0.2779(2)	0.3(1)
Ni	6c	1.0	0	0	0.3873(2)	0.3(2)
Ni	3b	1.0	0	0	1/2	0.9(3)

[a]Space group: $R\bar{3}m$ (No. 166), a = 0.49831(9) nm and c = 3.6136(5) nm. R_{wp} = 13.5%, R_I = 6.4%, R_e = 8.1%, and S = 1.6.

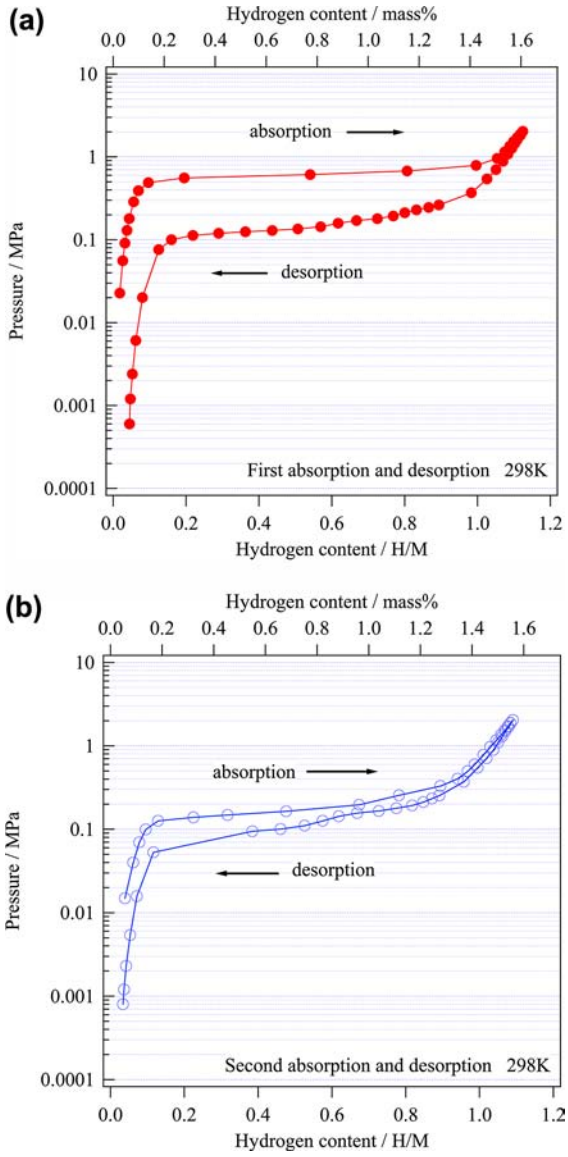

Figure 4. P–C isotherm of Pr_3MgNi_{14} at 298 K: (a) first absorption–desorption process and (b) second absorption–desorption process.

evacuated at 413 K for 1 h. In the second absorption–desorption measurement, the absorption plateau decreased to 0.16 MPa in comparison with the first absorption process and the Hf value was 0.47. The plateau region and the maximum hydrogen capacity were similar to those of the first absorption–desorption process.

3.3. Cyclic Absorption–Desorption Property of Pr_3MgNi_{14}.

The cyclic property of Pr_3MgNi_{14} up to 1000 cycles was investigated using a P–C isotherm machine at 313 K, and the results are shown in Figure 5. The retention rate was

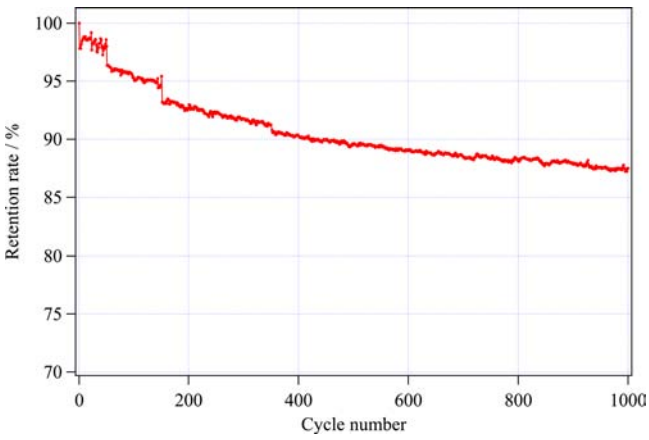

Figure 5. Cyclic absorption–desorption property of Pr_3MgNi_{14} at 298 K.

evaluated using the maximum hydrogen capacity divided by the value of the initial cycle. The decrease of the retention rate was steep up to 400 cycles, then levels out after 400 cycles. The retention rate decreased to 90.3% at 400 cycles and to 87.5% after 1000 cycles.

3.4. Crystal Structure Analysis after 1000 Cycles.

Figure 6 shows the Rietveld refinement pattern of Pr_3MgNi_{14} after 1000 absorption–desorption cycles. A two-phase model, which included the Gd_2Co_7-type and $PuNi_3$-type structures, was adopted for the Rietveld refinement. The model is the same as that of the alloy before hydrogenation. The pattern was

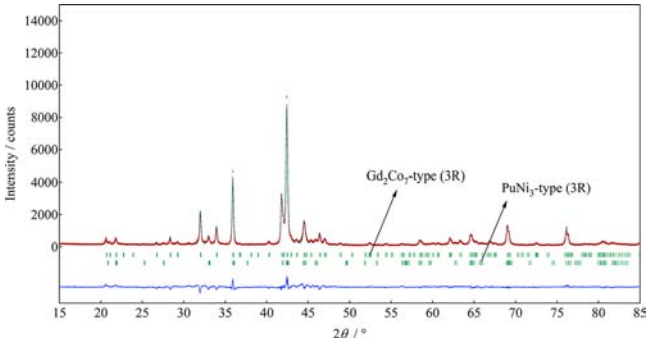

Figure 6. Rietveld refinement of XRD data after 1000 absorption–desorption cycles.

dx.doi.org/10.1021/ic301743p | Inorg. Chem. 2012, 51, 11805–11810

refined using profile parameters, including the anisotropic broadening parameters X_e (crystallite size) and Y_e (lattice strain), and isotropic parameters. The *S*-value was 2.1 and a satisfactory fit was obtained. The refined lattice parameters of the Gd_2Co_7-type structure were a = 0.4992(1) nm and c = 3.6591(7) nm, which were larger than those of the alloy before hydrogenation. The same tendency was also seen for the $PuNi_3$-type phase; the refined lattice parameters were a = 0.4994(1) nm and c = 2.4331(5) nm. Expansions of lattice parameters a and c, the unit-cell volume V, the length along the c-axes of the $PrNi_5$ and $PrMgNi_4$ cells, and the volume of the $PrNi_5$ and $PrMgNi_4$ cells in the Gd_2Co_7-type and $PuNi_3$-type structures after the initial cycle and 1000 cycles are shown in Tables 2 and 3. Expansions of the $PrNi_5$ and $PrMgNi_4$ cells in the c-axes of the $PrMgNi_4$ and $PrNi_5$ cells are 5.52% and 2.53%, respectively.

Table 2. Expansions of Lattice Parameters, the Unit-Cell Volume, the Length along *c*-Axes of the $PrNi_5$ and $PrMgNi_4$ Cells, and the Volume of the $PrNi_5$ and Pr_3MgNi_{14} Cells after Initial Cycle

	expansion (%) after initial cycle	
	Gd_2Co_7-type	$PuNi_3$-type
a	0.27	0.21
c	0.72	0.62
V	1.26	1.04
c ($PrNi_5$ cell)	0.02	0.00
c ($PrMgNi_4$ cell)	2.89	−2.56
V ($PrNi_5$ cell)	0.57	0.42
V ($PrMgNi_4$ cell)	3.45	−2.15

Table 3. Expansions of Lattice Parameters, the Unit-Cell Volume, the Length along *c*-Axes of the $PrNi_5$ and $PrMgNi_4$ cells, and the Volume of the $PrNi_5$ and Pr_3MgNi_{14} Cells after 1000 Absorption−Desorption Cycles

	expansion (%) after 1000 cycles	
	Gd_2Co_7-type	$PuNi_3$-type
a	0.20	0.26
c	1.26	0.94
V	1.66	1.47
c ($PrNi_5$ cell)	0.07	2.44
c ($PrMgNi_4$ cell)	3.28	−0.60
V ($PrNi_5$ cell)	0.47	2.98
V ($PrMgNi_4$ cell)	3.68	−0.08

the Gd_2Co_7-type structure after 1000 cycles were 0.47% and 3.68%, respectively. The $PrMgNi_4$ cell was expanded ∼8 times larger than the $PrNi_5$ cell.

4. DISCUSSION

4.1. Crystal Structure of R_3MgNi_{14}. Pr_2Ni_7 has a hexagonal Ce_2Ni_7-type structure at high temperature and a rhombohedral Gd_2Co_7-type structure at low temperature.[17,18] The high-temperature phase exists up to 1433 K, as shown in the Pr−Ni phase diagram.[19] In this study, the Pr_3MgNi_{14} ingot was annealed at 1343 K for 10 h under an argon atmosphere. However, the main phase was determined by Rietveld refinement to be Pr_3MgNi_{14}, with the Gd_2Co_7-type structure. The lattice parameters of Gd_2Co_7-type Pr_2Ni_7 are a = 0.5015 nm and c = 3.664 nm.[17] The effect of Mg substitution on the Pr_2Ni_7 lattice is the change of the lattice parameters by Δa = −0.64% and Δc = −1.38%; the shrinkages of the length along

α-La_2Ni_7, with the Ce_2Ni_7-type structure (low-temperature form), transforms to β-La_2Ni_7 with the Gd_2Co_7-type structure (high-temperature form) at 1249 ± 3 K.[20] β-La_2Ni_7 exists from 1251 K to 1287 K. Denys et al. reported the crystal structure of La_3MgNi_{14} annealed at 1023 K for 4 days.[21] The alloy was identified as La_3MgNi_{14}, with the Ce_2Ni_7-type structure. The Rietveld refinement on the XRD data was conducted based on the Ce_2Ni_7-type model, in which the Mg atoms were located only at the La1 site in the A_2B_4 cell. The refined lattice parameters of the alloy were a = 0.502822(7) nm and c = 2.42032(6) nm. The present authors previously reported the lattice parameters of α-La_2Ni_7 as a = 0.50656(9) nm and c = 2.4714(3) nm.[3] The effect of Mg substitution on the La_2Ni_7 lattice is the change of Δa = −0.74% and Δc = −2.07%; the shrinkages of the length along the c-axes of the $LaMgNi_4$ and $LaNi_5$ cells were 5.32% and 2.59%, respectively. The result is similar to that of Pr_3MgNi_{14}, although the crystal structures of R_3MgNi_{14} are different between R = Pr and R = La.

Zhang et al. reported the crystal structure and the first principal calculation of $(Nd_{1.5}Mg_{0.5})Ni_7$.[22] From the XRD measurement, the 2H- and 3R-type A_2B_7 structures coexisted in the $(Nd_{1.5}Mg_{0.5})Ni_7$. The phase abundance of 3R-type increased with decreasing the average A-atomic radius. From the Rietveld refinement, Mg atoms occupy the Nd sites in the A_2B_4 cell. The total energy of $(Nd_{1.5}Mg_{0.5})Ni_7$ with various site-occupation configuration for Mg atoms was determined by the first principal calculation. The total energy of $(Nd_{0.5}Mg_{0.5})_2Ni_4$ cell and $(Nd_{0.5}Mg_{0.5})Ni_5$ cell was −195.273 eV and −193.011 eV, respectively. Mg atoms prefer to occupy Nd sites in Nd_2Ni_4 cell, which agreed with the XRD results. In our study, the Pr_3MgNi_{14} has the 3R-type A_2B_7 structure by XRD. The 3R structure may stabilize with decreasing the average A-atomic radius. Mg atoms occupy Pr sites in A_2B_4 cell. The metal sublattice of the Pr_3Mg Ni_{14} was deformed anisotropically by the Mg substitution. It is expected that the total energy of the $PrMgNi_4$ cell is smaller than that of the $PrNi_5$ cell.

4.2. Hydrogenation Properties. The *P*−*C* isotherms of $LaNi_5$ at 303 K for the five absorption−desorption cycles were investigated by Inui et al.[23] The absorption pressure decreased from 0.9 MPa for the first cycle to 0.3 MPa for the second cycle, while the desorption pressure was kept at ∼0.2 MPa. The second absorption pressure decreased by 67% from the first absorption pressure. The *P*−*C* isotherms of Pr_3MgNi_{14} at 298 K are shown in Figures 4a and 4b. A wide plateau region is observed in the first and second absorption−desorption processes. The second absorption pressure decreased by 74% from the first one.

Goodell investigated the cyclic hydrogenation property of $LaNi_5$ during 1500 absorption−desorption cycles at 358 K.[24] The hydrogen capacity was reduced from 0.88 H/M for the initial cycle to 0.72 H/M for the 1000 cycles, and the retention rate was reduced to 82%. In the present study, the retention rate of Pr_3MgNi_{14} was 87.5% after 1000 absorption−desorption cycles, which compares favorably with that of $LaNi_5$.

Liu et al. reported crystal structures and cyclic hydrogen absorption−desorption stability of $(La,Mg)_5Ni_{19}$.[9] The alloy is composed of multiple phases with mass fractions of 46% Pr_5Co_{19}-type (2H), 18% Ce_5Co_{19}-type (3R), 31% $CaCu_5$-type, and 5.3% Ce_2Ni_7-type (2H) phases. The cyclic absorption−desorption properties were investigated up to 30 cycles at 343

dx.doi.org/10.1021/ic301743p | Inorg. Chem. 2012, 51, 11805−11810

K. The retention rate of $(La,Mg)_5Ni_{19}$ was 89% at 30 cycles, which should be compared to 98% of Pr_3MgNi_{14} at 30 cycles.

4.3. Expansion of the Crystal Lattice. Table 2 shows expansions of the lattice parameters, the unit cell, the length along the *c*-axes of the $PrNi_5$ and $PrMgNi_4$ cells, and the volume of the $PrNi_5$ and $PrMgNi_4$ cells of the Gd_2Co_7-type and $PuNi_3$-type structures, respectively, after the initial cycle. The metal sublattice of both the Gd_2Co_7-type and the $PuNi_3$-type structures expanded anisotropically along the *c*-axis. In particular, *c* of the $PrMgNi_4$ cell shows an increase in the Gd_2Co_7-type structure, while it decreases in the $PuNi_3$-type structure. In addition, the expansion of the $PrMgNi_4$ cell of the Gd_2Co_7-type structure was 3.45%, while that of the $PuNi_3$-type structure was −2.15%. There are no large differences in the expansion of lattice parameters *a* and *c*, the unit-cell volume, or the $PrNi_5$ cell between the Gd_2Co_7-type and $PuNi_3$-type. The expansion of the crystal lattice after 1000 cycles of hydrogen absorption−desorption is shown in Table 3. The results are similar to the results obtained after the initial cycle.

4.4. Lattice Strain. The lattice strain gives rise to the Bragg peak broadening. The phenomenon has been analyzed by Klug and Warren,[25,26] and with the Rietveld analysis software RIETAN 2000,[13,14] it is possible to analyze the lattice strain.

Nakamura and Akiba reported the lattice strain of $LaNi_5$ in the first hydrogen absorption−desorption process by in situ XRD.[27] The lattice strain during the hydrogen absorption−desorption process was investigated by investigating the peak broadening in the Rietveld analysis. The peak broadening was observed both in the 1st cycle and the 1000th cycle. The refined isotropic strain parameter (U) and anisotropic strain parameter (Y_e) were used for the measures of anisotropic and isotropic strains. The anisotropic broadening vector was determined to be ⟨110⟩ and the anisotropic lattice strain was determined to be 1.9% after the first activation process. The value of *U* increased to 0.238 with increasing hydrogen content, which corresponds to 0.5% of isotropic strain. After 1000 cycles, the anisotropic broadening vector was determined to be ⟨110⟩ and the anisotropic and isotropic lattice strains were 2.1% and 1.1%, respectively.

The anisotropic and isotropic strains of the Gd_2Co_7-type phase in Pr_3MgNi_{14} were refined using the parameters Y_e and *U*. The anisotropic broadening vector was determined to be ⟨001⟩. The anisotropic and isotropic lattice strains were determined to be 0.3% and 0.1% after the first activation process, values which are smaller by one order of magnitude than those of $LaNi_5$. Pr_3MgNi_{14} consists of cells with $PrMgNi_4$ and $PrNi_5$stacked along the *c*-axes in ratios of 1:2. The $PrNi_5$ cells relax the lattice strain of the $PrMgNi_4$ cells along the *c*-axes. After 1000 cycles, the anisotropic and isotropic lattice strains were 0.2% and 0.1%, respectively, which do not differ significantly from those after the first activation process. The results mean that both anisotropic and isotropic lattice strains are formed quickly and saturated at the first activation process. The same tendency was also seen in the $PuNi_3$-type phase in Pr_3MgNi_{14}. Thus, the cyclic hydrogen absorption−desorption property of Pr_3MgNi_{14} is better than that of $LaNi_5$, which is probably caused by the lattice strain formed in the first activation process.

5. CONCLUSIONS

We investigated crystal structures and the cyclic hydrogen absorption−desorption property of Pr_3MgNi_{14}. From the Rietveld refinement, it was shown that the present sample consisted of two phases: 80% Gd_2Co_7-type and 20% $PuNi_3$-type. For the Gd_2Co_7-type structure, the Mg atoms were located only at the Pr1 site in the A_2B_4 cell. The refined lattice parameters of the Gd_2Co_7-type structure were a = 0.49831(9) nm and c = 3.6136(5) nm.

The *P*−*C* isotherm of Pr_3MgNi_{14} showed a wide plateau and reversible hydrogenation properties. The maximum hydrogen capacity reached 1.12 H/M (1.61 mass %) at 298 K. The cyclic hydrogenation property compares favorably with $LaNi_5$; the retention rate of Pr_3MgNi_{14} was 87.5% after 1000 absorption−desorption cycles.

After the first hydrogenation, the metal sublattice of the Gd_2Co_7-type structure expanded anisotropically along the *c*-axis. The expansions of the $PrNi_5$ and $PrMgNi_4$ cells were, respectively, 0.57% and 3.45% from the original alloys. Similar results were observed after 1000 absorption−desorption cycles. The anisotropic and isotropic lattice strains of Pr_3MgNi_{14} were smaller than those of $LaNi_5$ during cyclic testing. These strains of Pr_3MgNi_{14} were almost saturated at the first cycle and remained constant after 1000 cycles.

AUTHOR INFORMATION

Corresponding Author

*Tel.: +81-29-287-7189. Fax: +81-29-287-7189. E-mail address: fbiwase@mx.ibaraki.ac.jp.

Notes

The authors declare no competing financial interest.

ACKNOWLEDGMENTS

The authors thank Emeritus Professor H. Asano (University of Tsukuba) for helpful advice.

REFERENCES

(1) Verbetsky, V. N.; Klyamkin, S. N.; Kovriga, A. Yu.; Bespalov, A. P. *Int. J. Hydrogen Energy* **1996**, *21*, 997−1000.
(2) Denys, R. V.; Yartys, V. A.; Sato, M.; Riabov, A. B.; Delaplane, R. G. *J. Solid State Chem.* **2007**, *180*, 2566−2576.
(3) Iwase, K.; Sakaki, K.; Nakamura, Y.; Akiba, E. *Inorg. Chem.* **2010**, *49*, 8763−8768.
(4) Yamamoto, T.; Inui, H.; Yamaguchi, M.; Sato, K.; Fujitani, S.; Yonezu, I.; Nishio, K. *Acta Mater.* **1997**, *45*, 5213−5221.
(5) Iwase, K.; Mori, K.; Hoshikawa, A.; Ishigaki, T. *Inorg. Chem.* **2011**, *50*, 11631−11635.
(6) Yasuoka, S.; Magari, Y.; Murata, T.; Tanaka, T.; Ishida, J.; Nakamura, H.; Nohma, T.; Kihara, M.; Baba, Y.; Teraoka, H. *J. Power Sources* **2006**, *156*, 662−666.
(7) Zhang, Q.; Fang, M.; Si, T.; Fang, F.; Sun, D.; Ouyang, L.; Zhu, M. *J. Phys. Chem. C* **2010**, *114*, 11686−11692.
(8) van Vucht, J. H. N.; Kuijpers, F. A.; Bruning, H. C. A. M. *Philips Res. Rep.* **1970**, *25*, 133−140.
(9) Liu, Z. Y.; Yan., X. L.; Wang, N.; Chai, Y. J.; Hou, D. L. *Int. J. Hydrogen Energy* **2011**, *36*, 4370−4374.
(10) Nakamura, J.; Iwase, K.; Hayakawa, H.; Nakamura, Y.; Akiba, E. *J. Phys. Chem. C* **2009**, *113*, 5853−5859.
(11) Nakamura, Y.; Oguro, K.; Uehara, I.; Akiba, E. *J. Alloys Compd.* **2000**, *298*, 138−145.
(12) Iwase, K.; Sakaki, K.; Matsuda, J.; Nakamura, Y.; Ishigaki, T.; Akiba, E. *Inorg. Chem.* **2011**, *50*, 4548−4552.
(13) Izumi, F. *Rigaku J.* **2000**, *17*, 34−45.
(14) Izumi, F. *The Rietveld Method*; Young, R. A., Ed.; International Union of Crystallography (Oxford University Press): Oxford, U.K., 1993; p 13.
(15) Larson, A. C.; Von Dreele, R. B. *GSAS-General Structure Analysis System*, Report No. LAUR 86-748, Los Alamos National Laboratory, Albuquerque, NM, 1994 ; pp 127−138.

(16) Bish, D. L. *Modern Powder Diffraction, Reviews of Mineralogy*, Vol. *20*; Post, J. E., Ed.; Mineralogical Society of America: Washington, DC, 1989.
(17) Virkar, A. V.; Raman, A. *J. Less-Common Met.* **1969**, *18*, 59−66.
(18) Buschow, K. H. J.; Van Der Goot, A. S. *J. Less-Common Met.* **1970**, *22*, 419−428.
(19) *Binary Alloy Phase Diagrams*, 2nd Ed., plus updates; Okamoto, H., Ed.; ASM International: Materials Park, OH, 1990.
(20) Zhang, D.; Tang, J.; Gschneidner, K. A. *J. Less-Common Met.* **1991**, *169*, 45−53.
(21) Denys, R. V.; Riabov, B.; Yartys, V. A.; Delaplane, R. G.; Sato, M. *J. Alloys Compd.* **2007**, *446*−*447*, 166−172.
(22) Zhang, Q.; Zhao, B.; Liu, C.; Hu, Q.; Fang, F.; Sun, D.; Ouyang, L.; Zhu, M. *Inorg. Chem.* **2012**, *51*, 2976−2983.
(23) Inui, H.; Yamanoto, T.; Hirota, M.; Yamaguchi, M. *J. Alloys Compd.* **2007**, *330*−*332*, 117−124.
(24) Goodell, P. D. *J. Less-Common Met.* **1984**, *99*, 1−14.
(25) Klug, H. P.; Alexander, L. E. *X-ray Diffraction Procedures*; Wiley− Interscience: Hoboken, NJ, 1974.
(26) Warren, B. E. *X-ray Diffraction*; Dover Publications: New York, 1990.
(27) Nakamura, Y.; Akiba, E. *J. Alloys Compd.* **2000**, *308*, 309−318.